Front. Optoelectron. 2014, 7(3): 376–384
DOI 10.1007/s12200-013-0384-0

RESEARCH ARTICLE

Large group-index bandwidth product empty core slow light photonic crystal waveguides for hybrid silicon photonics

Charles CAER, Xavier LE ROUX, Samuel SERNA, Weiwei ZHANG, Laurent VIVIEN, Eric CASSAN (✉)

Institut d'Electronique Fondamentale, University Paris-Sud, CNRS UMR 8622, Bât. 220, 91405 Orsay Cedex, France

Abstract This paper investigates the slow light propagation in silicon on insulator wide slot photonic crystal waveguides (PCWs). Two design schemes are presented, relying on the dispersion engineering of hole lattice and slot, respectively. Mode patterns and band diagrams are calculated by 3D-plane wave expansion method. Then, coupling and slow light propagations are modeled using finite difference time domain method in a full Mach-Zehnder interferometer (MZI). Results show high amplitudes interference fringes and high coupling efficiencies. Fabrication and measurement of devices lead to slow light propagation with group indices above 50, while multiple scattering and localized modes near the band edge also observed. This study provides insights for losses in hollow core slot high group index waveguides.

Keywords silicon photonics, photonic crystals (PC), slot waveguides, slow waves

1 Introduction

The continuous development of silicon photonics has been motivated by the urge to catch up with complementary metal oxide semiconductor (CMOS) scaling in integrated circuits and the increasing data streams in optical interconnects throughout the last decade. To attain this objective, it is necessary to minimize the footprint of photonic circuits as much as possible. This challenge can be addressed by photonic crystals (PC) operating in slow light regime [1] or using micro-nano-cavities [2]. The slow light regime exhibits peculiar features such as the spatial compression of pulses flowing through PC waveguides resulting in a significant increase of the localized electromagnetic energy, beneficial for nonlinear optics and electro-optical modulation effects [3]. On the other hand, when a slow mode is located at the edge of the first Brillouin zone (FBZ), the group velocity dispersion dramatically increases, which makes the pulses broaden and distorted in time domain. Additionally, a high group index can induce backscattering and coupling losses, which are severe drawbacks to the generalization of devices functioning in the slow light regime. However, this problem has been partially addressed by a careful dispersion engineering, which allows maintaining a constant group index over a certain bandwidth by modifying the holes' array with holes' displacements or tuning of holes' radii [4–7]. Such dispersion engineering can cancel the group velocity dispersion [8], more importantly, can also probably reduce the losses to a simple $\times n_g$ dependence [9]. As shown in Ref. [10], the backscattering losses arising from the slow light regime have in fact much more impact on the signal than the group velocity dispersion (GVD).

To improve the functionality of photonic devices, some useful properties, such as light emission and nonlinear optical effects with low pump powers, are limited in silicon due to its indirect bandgap and relatively high efficiency of multi-photon absorption processes. In this context, the introduction of a slot in the waveguide provides a route to confine light in the low index material due to the strong discontinuity at the index contrast interface [11]. Chosen according to its second and third order nonlinear susceptibilities $\chi^{(2)}$ and $\chi^{(3)}$, the low index material can dramatically enhance the nonlinear effects in the photonic crystal waveguides (PCWs). $\chi^{(2)}$ electro-optic modulation [12] in slotted PC and $\chi^{(3)}$ four-wave mixing in slot waveguides [13] have been for example successfully demonstrated. But slotted waveguides can be also very useful for sensing applications thanks to the possible infiltration of the slot and because the analytes can then interact with the extrema of the electric field and not only with its evanescent part [14].

The introduction of a slot in the channel of a PCW

Received October 15, 2013; accepted November 6, 2013

E-mail: eric.cassan@u-psud.fr

modifies the band diagram by pulling the fundamental mode of the slot within the photonic bandgap [15] with a positive slope in the FBZ. Nevertheless, it is also possible to maintain the W1-defect line mode in the photonic bandgap by either modifying the width of the line defect or the slot width itself. The intrinsic slot mode has a similar behavior to the standard W1-defect line mode: it is index guided far from the edge of the FBZ, but becomes gap guided when it reaches the edge of the FBZ due to the anticrossing with the air band. Both modes can be excited with a photonic wire, depending on the waveguide geometry.

Owing to these properties, we explore in this paper the slow light characteristics of silicon on insulator (SOI) slot photonic crystal (SPCW) and comb photonic crystal waveguides (CPCW) (Fig. 1).

We reported in our previous works on dispersion engineered CPCW [16] and measurements of slow light in a Mach-Zehnder interferometer (MZI) and losses at group index values around 30 [17], but we did not focus on the coupling issues arising from the slow light propagation nor the mechanisms of losses in such waveguides. We propose in this paper to extend our dispersion engineering method to the two types of slotted PCWs, numerically investigate the slow light behavior in such waveguides, and then report experimental results on slow light in these waveguides. We conclude by discussing on the mechanism of losses and give some clues for future investigation of losses in these types of slotted PCW.

This paper is divided as follows: in Section 2, we present plane wave expansion (PWE) calculations devoted to dispersion engineering in both SPCW and CPCW. We show in Section 3 by finite difference time domain (FDTD) simulations of a complete device that the slow modes exhibited by PWE method are not hindered by the coupling with a photonic wire, and we observe strong interference fringes and a clear slow light behavior when exciting a CPCW with a continuous wave (CW) source.

Experimental measurements of slow light are then reported in Section 4, confirming the simulated spectrum in both waveguides, before concluding in Section 5.

2 Model for slow light

2.1 Structure and method

The issue explored in this paper is the way to obtain SPCW operating in a flat band slow light regime while having a wide slot ($>$140 nm). We report here a methodology to achieve this statement by the introduction of Bragg-like corrugations to the slot, similar to a Bragg grating but which provides three additional degrees of freedom and allows tailoring the guided mode in order to obtain flat band group index curves. It is also shown that these corrugations ensure a stronger confinement of the electric field in the longitudinal direction. In the rest of the paper, we refer to the "W1" mode as the standard W1-defect line mode and to the "slot" mode as the fundamental mode of slot waveguides, as illustrated in Fig. 2. We realized dispersion engineering on the two modes, because the "W1" mode presents an easier coupling from a strip waveguide due to its mode profile. This mode is guiding light when the slot is narrow, whereas the "slot" mode is relevant when the slot is very large, which can be required in applications such as sensing in aqueous media [14].

The SPCW modes' profiles are obtained with the PWE method using the MIT Photonic Bandgap software [18] for a quasi- transverse electric (TE) polarization. Eigenmodes are calculated by the unit cell depicted in Fig. 2(c). It consists in a SOI slab with a buried oxide layer and a low index material cladding layer (e.g., polymer or liquid),

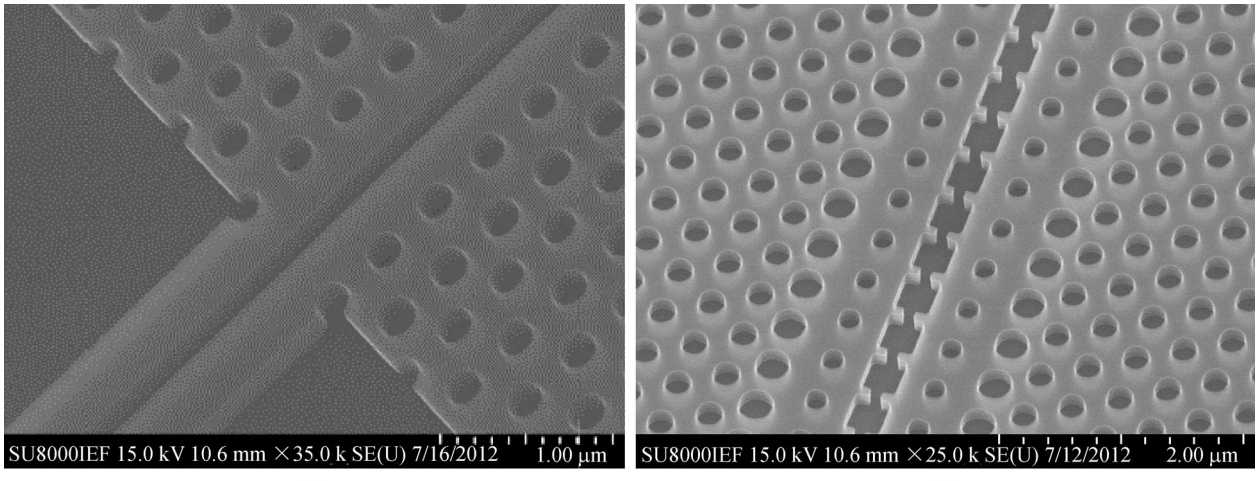

(a) (b)

Fig. 1 (a) Scanning electron microscope (SEM) image of a SPCW; (b) SEM image of a CPCW

whose indices are $n_{\text{Silicon}} = 3.48$, $n_{\text{Silica}} = 1.44$ and $n_{\text{Cladding}} = 1.46$, respectively. The slab thickness h is 220 nm, the lattice constant $a = 400$ nm, and the hole radius r is 110 nm to ensure a wide TE bandgap. As pointed out in Ref. [16], the first task to begin with is to fix the value of the slot width (W_{slot}). To make the filling of the slot easier while keeping a high confinement, we choose slot widths around 140 nm. The nominal defect line cannot support the slot mode. Therefore, in order to maintain the mode within the photonic bandgap, we set the line defect to W1.25, i.e., $1.25\sqrt{3}a$.

2.2 Tuning "slot" mode

Starting from a W1.25 standard PCW without slot, we calculate the dispersion diagram for increasing values of W_{slot}, in order to evaluate the general shape of the "W1" mode, and find the suitable W_{slot} value to start with the "slot" mode from a flat dispersion curve under the light line. The dispersion curve is progressively flattened for increasing W_{slot} values, as the frequency values increase near the FBZ at $k = 0.5$.

We introduce corrugations on the slot as described in Fig. 2(c). Three parameters define the desired comb. Similarly to a Bragg grating waveguide, l is the duty cycle and dy is the depth of the grating. We also define dx as the displacement of the comb grating regards to the centers of the first hole row. It is important to note that the periodicity of the comb is exactly the same as the one of the PC. Therefore, the corrugations do not act like a Bragg grating which would introduce minibands, but provide the three additional degrees of freedom previously mentioned for dispersion engineering.

Increasing these three values shifts the frequencies up and allows careful dispersion engineering. The band can be fully engineered by combining it with a hole radius tuning. Results of group index of 55 and bandwidth of 5 nm are reported for example in Fig. 3. Referring to the definition of the group index bandwidth product (GBP):

$$\text{GBP} = \langle n_{\text{g}} \rangle \frac{\Delta\omega}{\omega_0},$$

where $\langle n_{\text{g}} \rangle$ stands for the average group index over a bandwidth $\Delta\omega$ and ω_0 the central wavelength, we obtain a GBP of 0.17. It has to be kept in mind that this GBP is not as large as in some previous studies [1,19] because of the cladding layer index considered here ($n_{\text{Cladding}} = 1.46$) which enlarges the light cone compared to an air cladding, thus reducing the available bandwidth. The obtained GBP is close to the theoretical limit, therefore provides a comfortable bandwidth with a large group index.

It appears that the electric field pattern is highly affected by the variation of dx. Indeed, a large value of l and setting $dx = 0$ (i.e., the center of the corrugation has the same value over the x axis as the center of the first holes) provides a strong confinement in the waveguide direction where the slot is narrowing (see Fig. 2). Although the "W1" mode is also engineered, it is not relevant to exploit it with this geometry, since the shape of the comb does not confine the energy within it.

2.3 Tuning "W1" mode

Similar dispersion engineering to those exposed in the previous section can be applied to tune the W1 defect mode that we called "W1" mode. As this mode comes from the defect along the PCW, it appeared to be less sensitive to the tailoring of the comb far from the air band. The procedure is the same: we start with the choice of an adequate slot width, then we tune the slope by changing the values of W2 and W3, and finally we tailor the comb. If we want to engineer the dispersion of a SPCW with a wide slot, it is better to work with a wider PCW channel, e.g., W1.4, but we lose the benefit of a strong localization of light at the

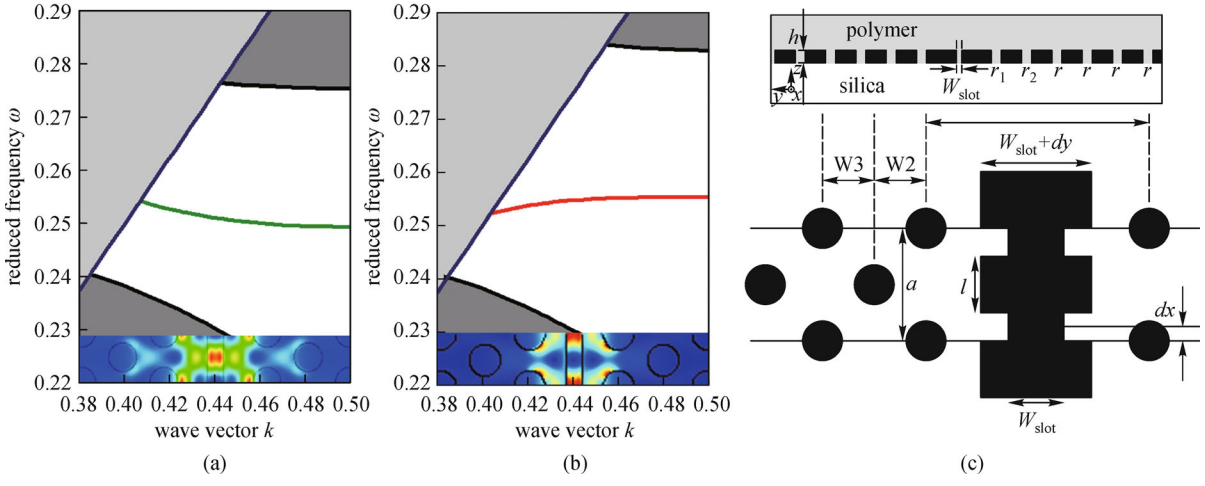

Fig. 2 (a) Even guided "W1" mode originating from the W1 line defect. Inset: $\varepsilon|E|^2$ pattern; (b) even guided "slot" mode coming from the slot waveguide. Inset: $\varepsilon|E|^2$ pattern; (c) unit cell implemented for PWE simulations with all parameters used for dispersion engineering

narrowing, and it is harder to tailor the hole "W1" mode which is more sensitive to the modification of the hole array. We thus maintained the PCW channel at W1.25, as this width still reduces the overlap between the optical mode and the holes.

The main effect of the corrugations on this mode acts throughout the parameter *dx*: as this parameter controls the position of the comb with respect to the hole array, its variation strongly modifies the electromagnetic field pattern. An optimum confinement is found when $dx = 0.5a$, as depicted in Fig. 4. This means that where the mode is naturally localized in the slot, adding a corrugation there will strongly reduce the mode volume by a factor depending roughly on the comb duty cycle l. We obtain a mean group index of 35 over a bandwidth of 6 nm, giving a GBP of 0.14.

3 Transmission coupling calculations

As calculations of SPCW have demonstrated a flat band slow light behavior in the previous section, it is interesting here to compute the transmission of an entire device in order to estimate the related coupling losses from/into strip input/output waveguides. The transmission spectrum of the PCW is obtained by the FDTD using the MIT electromagnetic equation propagation (MEEP) software [20]. The implemented structure (see Fig. 5) consists in a MZI with input and output waveguides. The *Y*-junction splits in two arms with two 90° bends and curvature radius of 5 µm. The reference arm is a 400 nm-width strip waveguide, while the signal arm contains the CPCW. In the signal arm, two stages ensure the conversion between the strip waveguides and the CPCW. This adaptation is critical due to the high mismatch between the mode of a Si strip waveguide and a slow mode of a SPCW in order to avoid severe reflection. First, the strip waveguide is converted into a slot waveguide by using the tapering section proposed in Ref. [21]. This robust design ensures a coupling efficiency higher than 90% on a length smaller than 15 µm. Then, the slot waveguide couples to fast modes of the CPCW. We estimate the reflection to be approximately 3 dB. The light finally enters the slow light section. The adaptation between the slow and the fast modes is done by stretching the lattice constant at the input and output of the PCW [22]. This simple design allows a high coupling efficiency close to unity even at high group indices. The lattice constant is 400 nm in the central section and then is 410 and 420 nm on five periods each. As a whole, the length of the PCW is 88.7 µm (200 periods in the slow light section), and the length of the complete structure with all sub-regions is 277.5 µm. The computational cell is wide enough to avoid coupling with the perfectly matched layers. The structure is implemented in 2D using the slab effective index approximation for practical reasons, as 3D in slow light regime requires a considerable amount of memory and calculation time. For example, a 80 µm long device wherein flows a pulse with a group index of 60 requires

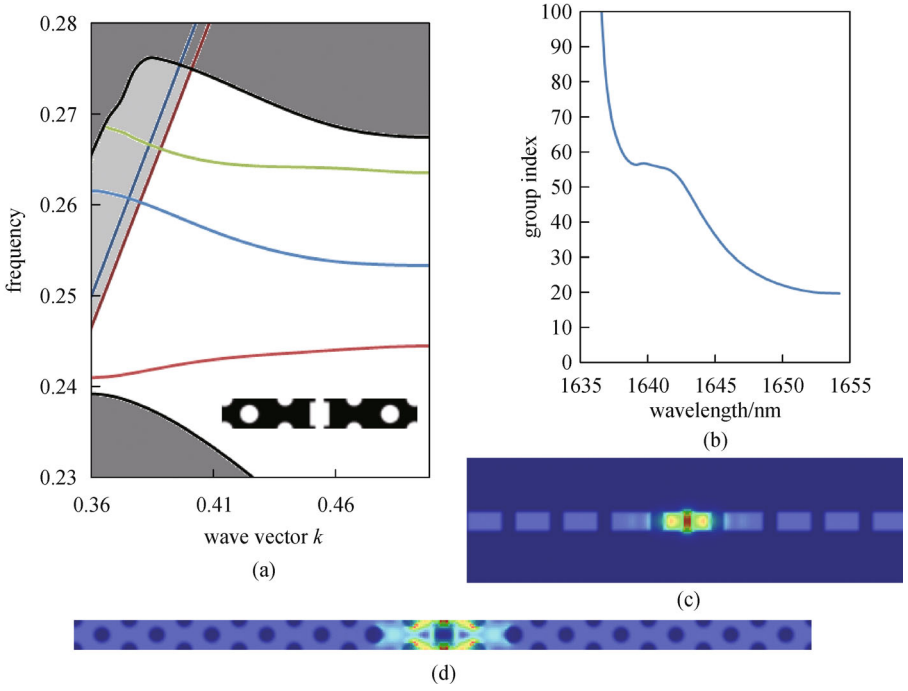

Fig. 3 (a) Band diagram of the engineered "slot" mode (red curve). Green curve is the "W1" mode and the blue one the odd mode.. Inset: Unit cell; (b) corresponding group index; (c) cross-section of the $\varepsilon|E|^2$ pattern at $k = 0.43$; (d) view of $\varepsilon|E|^2$ pattern in *xy* plane at $k = 0.43$. Parameters of structure are: W1.25, W2 = 0.65, W3 = 0.45, $W_{slot} = 0.2625a$, $dx = 0$, $dy = 0.35$a, $l = 0.8$, $r_1 = 0.25a$, $r_2 = 0.2875a$

a running time higher than 30000 time units (a/c). Therefore, 3D FDTD calculations in slow light regime are not sustainable. The effective index of the silicon is in the studied case 2.83. The simulation time range is 70 ps (i. e., 50000 c/a time units) and the source is a broadband Gaussian pulse centered at 1550 nm with a spectral width of 500 nm. The sensors have a resolution of 50 pm. The grid resolution is 20 nm per pixel. This represents a computation time of 50 h on 16 CPU. The parameters of the photonic crystal are W1.4, W2 = 0.65, W3 = 0.45, r_1 = 0.25a, r_2 = 0.38a, r = 0.3a, and those of the comb are W_{slot} = 0.4a, dy = 0.5a, dx = 0.5a, l = 0.75a. The group index dependence with respect to the bandwidth is extracted from the interference fringes as follows:

$$n_g^{sign} = n_g^{ref} + \frac{\lambda_{max}\lambda_{min}}{2L(\lambda_{max} - \lambda_{min})}. \quad (1)$$

The engineered SPCW has a "W1" mode with a group index plateau of 35 over 10 nm as shown in Fig. 5. The fringes amplitude is almost 25 dB, even close to the band edge, confirming the efficiency of the mode conversion and a low level of intrinsic losses and coupling losses. We also analyzed the slow light regime by exciting the CPCW with a continuous wave source at λ = 1621 nm, i.e., in the middle of the flat band slow light curve. For such an excitation, we observe a strong enhancement of the optical intensity and a light localization exactly at the position between the cladding grooves as predicted by the PWE method.

We underline here that the running time is a critical parameter for the observation of the interference fringes: indeed, physically, the slow pulse needs to reach the output in order to be detected by the sensor. This computation shows that it is possible to manipulate slow light by FDTD.

Arising from this confirmed high confinement of light within the comb, we can foresee a strong nonlinear effective area reduction, particularly if we operate at a pump power below the onset of nonlinearity of silicon but above the onset of nonlinearity of the nonlinear cladding layer. Moreover, we expect to dramatically reduce the mode volume in cavities with very narrow combs, which might be promising for cavity quantum electrodynamics [23].

4 Results and discussion

To complete our investigation of the presented SPCWs, We fabricated samples in the IEF/CTU-Minerve clean room. A 220 nm Si film with 2 μm of buried oxide SOITEC wafer has been processed. The pattern is formed in positive resist by the 80 kV e-beam lithography Nanobeam NB-4 system and then transferred by inductive coupling plasma (ICP) Reactive Ion Etching process. The facets of the sample are finally cleaved after removal of the resist. Before

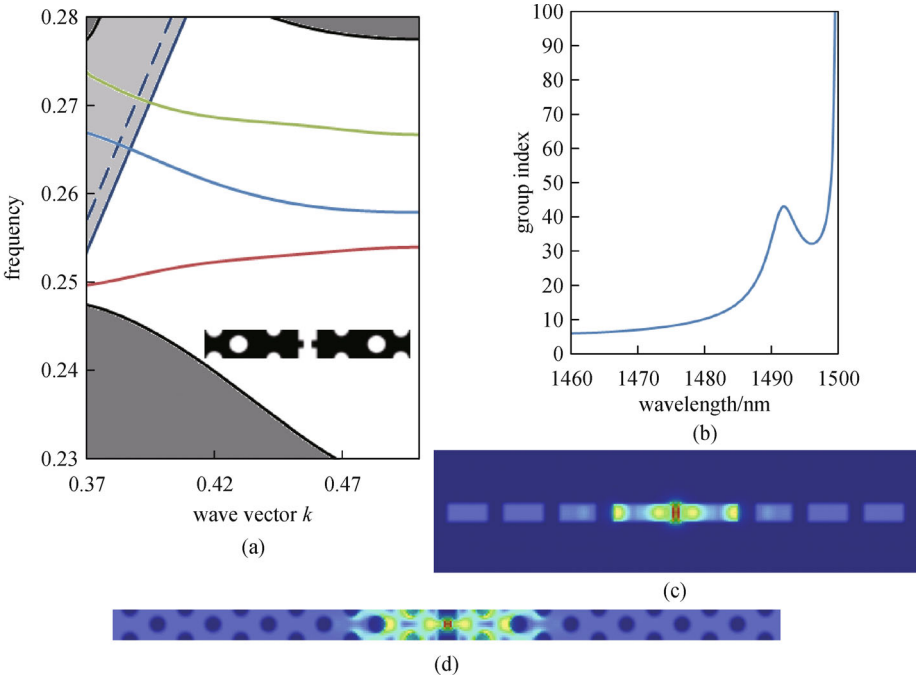

Fig. 4 (a) Band diagram of the engineered "W1" mode (green curve). Red curve is "slot" mode and the blue one is the odd mode. The dashed curve is silica light line. Inset: Unit cell; (b) corresponding group index; (c) cross-section of $\varepsilon|E|^2$ pattern at k = 0.43; (d) view of $\varepsilon|E|^2$ pattern in xy plane at k = 0.43. Parameters of structure are: W1.25, W2 = 0.65, W3 = 0.45, W_{slot} = 0.25a, dx = 0.5a, dy = 0.35a, l = 0.75, r_1 = 0.2325a, r_2 = 0.2875a

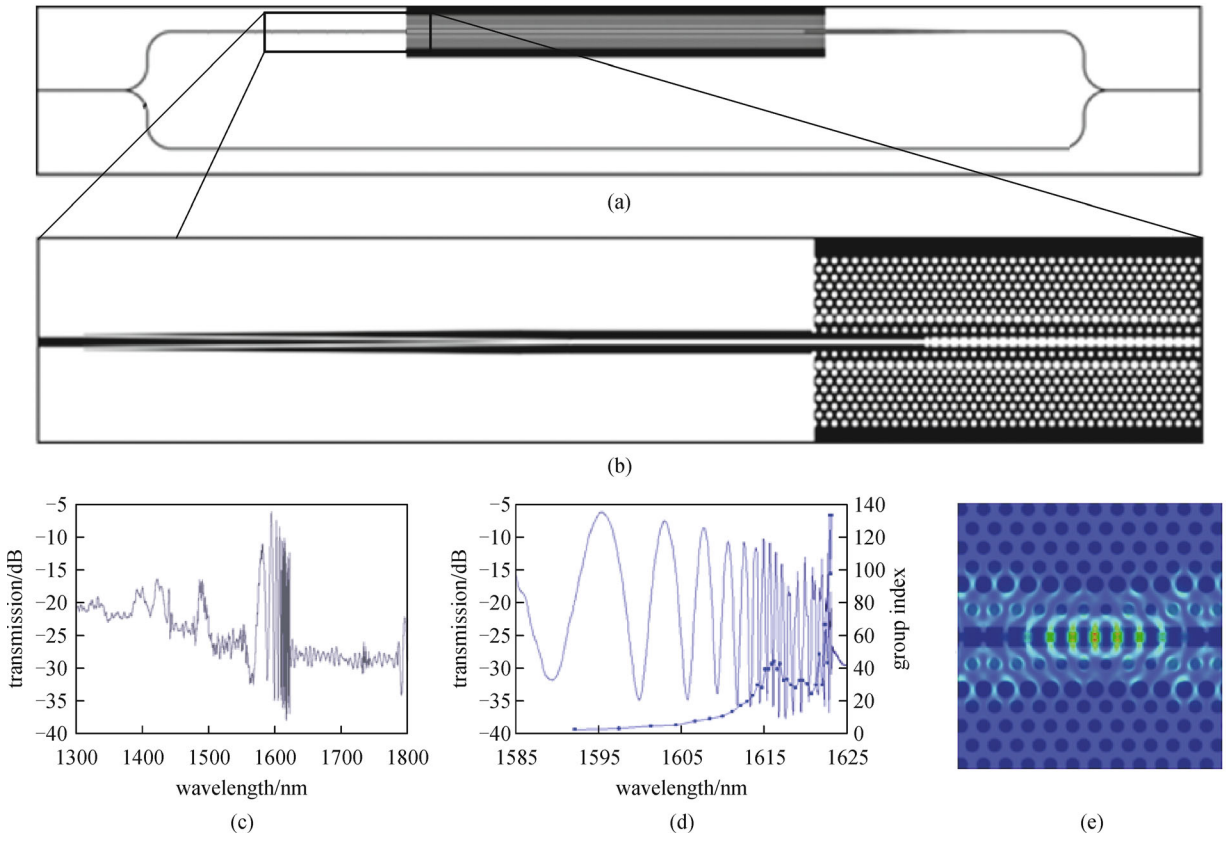

Fig. 5 (a) Representation of the simulated structure by FDTD; (b) detailed view of the input taper and the central part of the PCW; (c) transmission diagram of structure with strong interference fringes; (d) zoom on e interference fringes and calculated group index, exhibiting a flat band slow light; (e) $\varepsilon|E|^2$ pattern in photonic crystal for a continuous wave at $\lambda = 1621$ nm, confirming high confinement within comb

measurement, the surface of the sample is covered with a liquid whose refractive is 1.46, in order to symmetrize the structure. Due to the hydrophilic behavior of the silica and hydrophobic behavior of the silicon, we assume that the holes and the slots are fully infiltrated, since when inclining the sample by an angle of 90°, the liquid does not fall from the sample when we deposit a small droplet. The waveguides are probed by two tunable external cavity lasers (1390–1540 nm and 1520–1640 nm), where optical variable attenuators ensure the same power level for both sources. A polarization controller provides TE polarization, and a mono-mode tapered lensed fiber injects the light into a 3 µm strip waveguide. The input waveguide is adiabatically tapered into a 400 nm silicon nanowire through an 800 µm-long taper for single-mode operation. The 400 nm strip waveguide splits in two arms by a *Y*-junction with two 15° successive bends with radius R = 180 µm, these two arms forming a MZI. The total length of the MZI is approximately 500 µm. The reference arm is a strip waveguide and the signal arm contains the SPCW. The mode adaptation from the strip waveguide to the SPCW is ensured as explained in the previous section. Figure 6 shows different views of the fabricated structure. At the output, the transmitted power is collected by a microscope objective, and sent to an all-band optical component tester CT400 giving the optical transfer function.

The dimensions of the fabricated SPCW are: a = 400 nm, W1.25 = 870 nm, W2 = W3 = 345 nm, r = 112.5 nm, W_{slot} = 140 nm, dy = 100 nm, l = 0.7, and the length of the total SPCW is 92 µm. The transmission spectra plotted in Fig. 7 indicates a cut-off wavelength at $\lambda = 1521.5$ nm. The group index is extracted by analyzing the interference fringes as explained earlier. The reference being a strip waveguide, its group index is constant over the explored range of wavelengths and is roughly equal to 4. The Fourier transforms (FTs) of the transmission spectra are calculated, and by identifying the peaks on the FT spectrum, it is possible to remove those associated to Fabry-Perot noise of the sample facets with a low-pass filter, allowing more accurate extractions of the extrema of the interference fringes. Group indices are then measured in both devices up to a value around 60. This gives a group index bandwidth product of 0.07 when considering group indices higher than 15. The high amplitude of the fringes for group indices around 20 shows the low level of losses (Fig. 7).

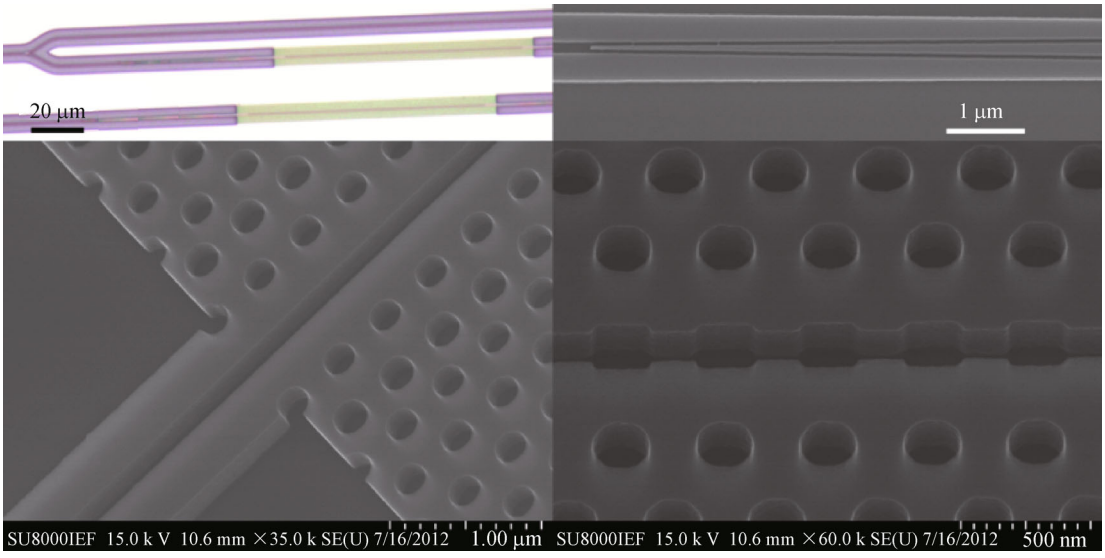

Fig. 6 From left to right and top to bottom: optical microscope view of the MZI and a SPCW, SEM micrograph of strip-to-slot taper, SEM micrograph of a SPCW, SEM micrograph of a CPCW

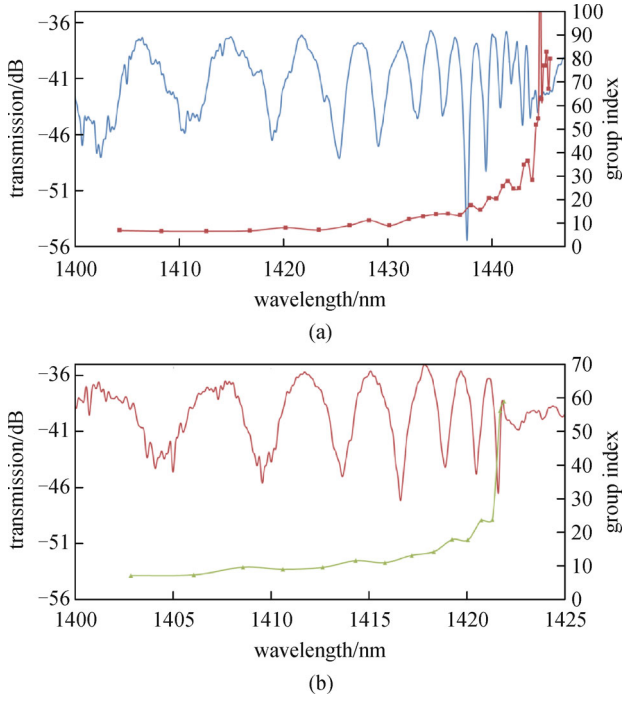

Fig. 7 (a) Transmission diagram of MZI containing a SPCW with extracted group indices from interference fringes; (b) transmission diagram of MZI containing a CPCW with extracted group indices from interference fringes

Figure 8 provides some hints on the loss mechanism in CPCW. Intensive studies on slow light have shown that the losses essentially arise from the fabrication induced disorder [24,25], where each defect acts as a scattering center. As long as this scattering point couples to a Bloch mode under the light line, light can be only either back scattered or forward scattered. But the scattered light can be scattered again by another defect. The disordered PCW starts then to behave like a Fabry-Perot cavity with a random resonant peak with a Q-factor that can be higher 20000 [26]. This suggests that this multiple scattering phenomenon is quite similar to the one experienced in standard W1 PCW, the difference likely residing in the correlation length of the defects.

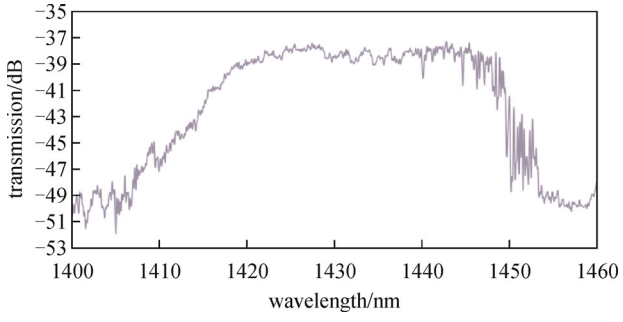

Fig. 8 Transmission spectrum of a 300 μm long CPCW. Disorder-induced multiple scattering arising from Anderson localization is clearly visible at the band edge

5 Conclusion

We have demonstrated that a comb PCW is a suitable structure for strongly confining light in a low index material. We showed that a proper dispersion engineering of the slot itself ensures a flat band group index curve, enabling a slow light operation over a sufficient bandwidth. We have presented two structures based on two different guided modes, operating in slow light regime with group indices of 55 and 35, over bandwidths of 5 and

6 nm, respectively, with slot widths above 140 nm. The slot enlargement is not realized at the expense of a low optical intensity, and the narrowing the slot into the comb presents interesting feature of a high localization of the electric field, which is of interest for configurations requiring small modal volume and nonlinear effective area. FDTD calculations showed an efficient mode conversion from the photonic wire to the SPCW and a high transmission near the band edge. The simulated structure shows slow light operation with a flat band group index of 35 over a bandwidth of 6 nm, and has very high amplitude of the interference fringes. The high localization of the electric field will offer a good opportunity for sensing devices and nonlinear optical effects.

We finally fabricated and measured SPCW and CPCW in integrated MZI. We have reported measurement of slow light with group indices up to 60 in both devices, while the amplitude of the interference fringes were around 10 dB, even at group indices around 20. The multiple scattering observed near the band edge gives an insight of the losses experienced in the slotted PCWs. A more precise model of loss will have to be investigated.

Acknowledgements The authors acknowledge financial support from the ANR POSIPLOT funding program. Charles Caër acknowledges a scholarship from the French Ministry of Higher Education and Research. The authors acknowledge Prof. Nicolas Dubreuil, Dr. Philippe Lalanne, Dr. Sylvain Combrié and Dr. Alfredo de Rossi for fruitful discussions.

References

1. Baba T. Slow light in photonic crystals. Nature Photonics, 2008, 2 (8): 465–473
2. Nozaki K, Shinya A, Matsuo S, Suzaki Y, Segawa T, Sato T, Kawaguchi Y, Takahashi R, Notomi M. Ultralow-power all-optical RAM based on nanocavities. Nature Photonics, 2012, 6(4): 248–252
3. Monat C, Corcoran B, Pudo D, Ebnali-Heidar M, Grillet C, Pelusi M D, Moss D J, Eggleton B J, White T P, O'Faolain L, Kauss T F. Slow light enhanced nonlinear optics in silicon photonic crystal waveguides. IEEE Journal of Selected Topics in Quantum Electronics, 2010, 16(1): 344–356
4. Frandsen L H, Lavrinenko A V, Fage-Pedersen J, Borel P I. Photonic crystal waveguides with semi-slow light and tailored dispersion properties. Optics Express, 2006, 14(20): 9444–9450
5. Kubo S, Mori D, Baba T. Low-group-velocity and low-dispersion slow light in photonic crystal waveguides. Optics Letters, 2007, 32 (20): 2981–2983
6. Hao R, Cassan E, Kurt H, Le Roux X, Marris-Morini D, Vivien L, Wu H M, Zhou Z P, Zhang X L. Novel slow light waveguide with controllable delay-bandwidth product and utra-low dispersion. Optics Express, 2010, 18(6): 5942–5950
7. Hao R, Cassan E, Le Roux X, Gao D S, Do Khanh V, Vivien L, Marris-Morini D, Zhang X L. Improvement of delay-bandwidth product in photonic crystal slow-light waveguides. Optics Express, 2010, 18(16): 16309–16319
8. Petrov A Y, Eich M. Zero dispersion at small group velocities in photonic crystal waveguides. Applied Physics Letters, 2004, 85(21): 4866–4868
9. O'Faolain L, Schulz S A, Beggs D M, White T P, Spasenović M, Kuipers L, Morichetti F, Melloni A, Mazoyer S, Hugonin J P, Lalanne P, Krauss T F. Loss engineered slow light waveguides. Optics Express, 2010, 18(26): 27627–27638
10. Mazoyer S, Baron A, Hugonin J P, Lalanne P, Melloni A. Slow pulses in disordered photonic-crystal waveguides. Applied Optics, 2011, 50(31): G113–G117
11. Xu Q F, Almeida V R, Panepucci R R, Lipson M. Experimental demonstration of guiding and confining light in nanometer-size low-refractive-index material. Optics Letters, 2004, 29(14): 1626–1628
12. Lin C Y, Wang X, Chakravarty S, Lee B S, Lai W, Luo J, Jen A K Y, Chen R T. Electro-optic polymer infiltrated silicon photonic crystal slot waveguide modulator with 23 dB slow light enhancement. Applied Physics Letters, 2010, 97(9): 093304-1–093304-3
13. Koos C, Vorreau P, Vallaitis T, Dumon P, Bogaerts W, Baets R, Esembeson B, Biaggio I, Michinobu T, Diederich F, Freude W, Leuthold J. All-optical high-speed signal processing with silicon-organic hybrid slot waveguides. Nature Photonics, 2009, 3(4): 216–219
14. Scullion M G, Di Falco A, Krauss T F. Slotted photonic crystal cavities with integrated microfluidics for biosensing applications. Biosensors & Bioelectronics, 2011, 27(1): 101–105
15. Di Falco A, O'Faolain L, Krauss T F. Photonic crystal slotted slab waveguides. Photonics and Nanostructures-Fundamentals and Applications, 2008, 6(1): 38–41
16. Caer C, Le Roux X, Do V K, Marris-Morini D, Izard N, Vivien L, Gao D S, Cassan E. Dispersion engineering of wide slot photonic crystal waveguides by bragg-like corrugation of the slot. IEEE Photonics Technology Letters, 2011, 23(18): 1298–1300
17. Caer C, Le Roux X, Cassan E. Enhanced localization of light in slow wave slot photonic crystal waveguides. Optics Letters, 2012, 37 (17): 3660–3662
18. Johnson S G, Joannopoulos J D. Block-iterative frequency-domain methods for Maxwell's equations in a planewave basis. Optics Express, 2001, 8(3): 173–190
19. Schulz S A, O'Faolain L, Beggs D M, White T P, Melloni A, Krauss T F. Dispersion engineered slow light in photonic crystals: a comparison. Journal of Optics, 2010, 12(10): 104004-1–104004-3
20. Oskooi A F, Roundy D, Ibanescu M, Bermel P, Joannopoulos J D, Johnson S G. A flexible free-software package for electromagnetic simulations by the FDTD method. Computer Physics Communications, 2010, 181(3): 687–702
21. Wang Z C, Zhu N, Tang Y B, Wosinski L, Dai D X, He S L. Ultracompact low-loss coupler between strip and slot waveguides. Optics Letters, 2009, 34(10): 1498–1500
22. Hugonin J P, Lalanne P, White T P, Krauss T F. Coupling into slow-mode photonic crystal waveguides. Optics Letters, 2007, 32(18): 2638–2640
23. Gao J, Gesuele F, Koh W K, Murray C B, Assefa S, Wong C W. Weak exciton-photon coupling of PbS nanocrystals in air-slot mode-gap Si photonic crystal nanocavities in the near-infrared. In: Proceedings of Lasers and Electro-Optics (CLEO) and Quantum Electronics and Laser Science Conference (QELS). San Jose, CA,

2010

24. Mazoyer S, Hugonin J P, Lalanne P. Disorder-induced multiple scattering in photonic-crystal waveguides. Physical Review Letters, 2009, 103(6): 063903-1–063903-4
25. Kuramochi E, Notomi M, Hughes S, Shinya A, Watanabe T, Ramunno L. Disorder-induced scattering loss of line-defect waveguides in photonic crystal slabs. Physical Review B: Condensed Matter and Materials Physics, 2005, 72(16): 161318-1–161318-4
26. Topolancik J, Vollmer F, Illic B. Random high-*Q* cavities in disordered photonic crystal waveguides. Applied Physics Letters, 2007, 91(20): 201102-1–201102-3